Modelling the Microstructure-dependent Fracture Toughness of Quenched and Tempered Martensitic Steels at Room Temperature

Since the testing of the plane strain fracture toughness (K_{IC}) is fairly complex and expensive by most standards, it is valuable to be able to determine K_{IC} on the basis of more readily obtained mechanical properties, such as those associated with a tensile test. A model using tensile test data, was originally proposed by Hahn and Rosenfield (HR) [1] describing a ductile fracture process controlled by micro-void coalescence. That model has been extended and implemented in JMatPro® v11 to determine K_{IC} for titanium and aluminium alloys at room temperature based on some critical microstructure information.

This report describes an extension of that capability to quenched and tempered high strength low-alloy (HSLA) martensitic steels, which is incorporated in the existing "Tempered Hardness" capability in JMatPro® v11. Martensitic steels show complexities of fracture mechanism(s) and both ductile fracture and brittle cleavage may appear as a result of tempering [2-4]. In this report, an additional model is used and combined with the HR model to capture the variation in fracture mechanism, thereby enabling reliable predictions of the room temperature K_{IC} of martensitic steels subject to different tempering conditions.

Microstructure and metallurgical findings

The fracture behaviour of a given structure or material depends on the stress level, presence of a flaw, material properties, and the mechanism(s) by which the fracture proceeds to completion. Since crack opening displacement decreases sharply with increasing strength, a basic trend of decreased toughness with increased strength has been identified. However, high-strength quenched and tempered martensitic steels may be embrittled following a short-time improper tempering treatment (~300ºC) [2-4], reflected as a reduction of fracture toughness as well as of the Charpy V-notch impact energy at this tempering condition.

A schematic is shown in Fig. 1, where the toughness can exhibit a non-monotonic evolution with increase in tempering temperature, different from the change of hardness or strength. This is often referred to as "tempered martensite embrittlement (TME)", with a single tempering treatment being sufficient to induce embrittlement. Another type of so-called temper embrittlement (TE) may occur above 400ºC but is understood to be noticeable only with excessive enhancing alloying elements, in particular, Cr and Ni. For HSLA considered in this report, TE is ignored and the embrittlement only refers to tempered martensite embrittlement (TME).

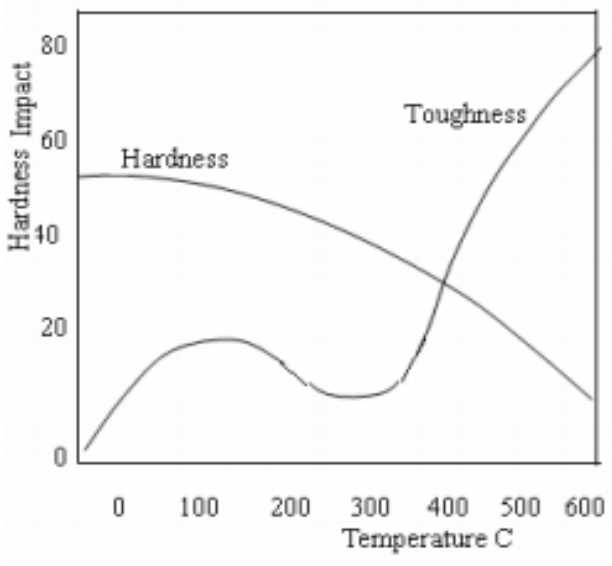

Figure 1. Schematic of change in hardness and room temperature fracture toughness of a quenched steel tempered for a short time at different temperatures

Tempered martensite embrittlement has been attributed to three major factors [2-4]. First, the embrittled condition coincides with the replacement of ε-carbides, a hardening phase typically obtained below 200°C tempering temperature, with more stable cementite precipitation. Second, segregation of impurity elements (e.g. S and P) to prior austenite grain boundaries during prior austenitisation is essential for embrittlement to occur. Third, the embrittling effect is concurrent with thermal and mechanical destabilisation of retained austenite which forms during cooling, generating brittle untempered martensite surrounded by tempered martensite. The degree of TME is thus dependent on a mixture of all these mechanisms. A considerable number of metallurgical findings of fractured surface have shown that the dominant fracture mode is by cleavage along the weakest path. However, despite these known factors, precise models to account for all aspects of TME have not been formulated yet [2].

Beyond the range of tempering temperature for TME, the main fracture morphology has been found to be ductile with dimples and micro-void coalescence, as well as some limited intergranular cracking [2-4]. Voids often nucleate at the interfaces between undissolved large inclusions and the matrix, where a stress concentration can be induced due to significant mismatch. These inclusions are understood to form mainly after austenitisation, for example, the typical manganese sulphide (MnS) in steels such as 4340 [2,5], as well as other large inclusions such as M(C,N) at relatively low austenitisation temperatures.

The deleterious role of S on toughness in steels is supported by the observed appreciable drop in the impact energy as S content increases [6]. However, it should be noted that removal of such impurity elements may not be feasible as it increases the cost of the final product, making it likely to be less competitive in the marketplace. In addition, S is sometimes deliberately added to certain commercial steel alloys to enhance their machinability.

The growth of initial large voids can be terminated prematurely by the development of void sheets—consisting of small voids—that link the large voids, while fractographic observations reveal that the small voids are attributed to fracture of coarse carbide particles found along martensite lath boundaries [2]. These coarse carbides are believed to precipitate mainly during the subsequent tempering, with the dominant phase being ε-carbide at low tempering temperatures (e.g. below 200°C) and cementite at high tempering temperatures (e.g. above 400°C) [3,4]. Morphology varies between the two phases, where ε-carbide mainly possesses needle shape [4,7] and cementite is mainly platelet or spherical [3,4]. As a consequence, toughness is expected to be dependent on the precipitate volume fraction and particle spacing.

Modelling the fracture mechanism transition

According to the microstructure and metallurgical observations, the following strategy is adopted to categorise the data and also to determine K_{IC} subject to different tempering temperatures:

- In the as-quenched condition, martensite is very brittle and is assumed to fracture by cleavage.
- Between room temperature and 200°C, a mixture of mechanisms is assumed but low temperature ductile micro-void coalescence gradually dominates towards 200°C due to the formation of ε-carbides.
- Between 200°C and 300°C, a mixture of mechanisms is assumed but cleavage gradually dominates towards 300°C due to the potential occurrence of tempered martensite embrittlement (TME).
- Between 300°C and 400°C, a mixture of mechanisms is assumed but high temperature ductile micro-void coalescence gradually dominates towards 400°C due to the formation of cementite.
- Above 400°C, high temperature ductile micro-void coalescence is assumed to fully control the fracture process.

Ductile fracture controlled by micro-void coalescence is captured by the HR model below.

$$K_{IC} \approx \sqrt{2E'\sigma_y n^2 \varepsilon_f} \quad (ksi\sqrt{in}) \qquad \text{or} \qquad K_{IC} \approx \sqrt{0.05 \cdot E'\sigma_y n^2 \varepsilon_f} \quad (MPa\sqrt{m}) \tag{1}$$

where E' is a correction of the elastic modulus for plane strain condition, $E' = E / (1-\upsilon^2)$, and υ is Poisson's ratio. σ_y is the yield strength at room temperature, n is the strain hardening exponent and ε_f is a critical fracture strain localized at the crack tip which must be exceeded by the local equivalent plastic strain over a characteristic distance in order for the catastrophic ductile fracture to occur.

The experimental K_{IC} values of a range of martensitic steels, along with E, υ, σ_y and n calculated by JMatPro®, are first substituted in Eq. (1) to back calculate ε_f. Based on an equivalent model proposed by Ritchie et al [8], ε_f can then be correlated to the diameter and mean spacing of void initiating particles (assumed to be spherical), as well as a characteristic distance. For martensitic steels, the void initiating particles mainly refer to the large precipitates formed after austenitisation (typically MnS and M(C,N)). The diameter and mean spacing can be reduced to one parameter, the volume fraction, according to a physical formulation given by Friedel [9]. The characteristic distance is assumed to be proportional to the mean inter-particle spacing of the dominant carbide phases formed during tempering. Taking into account the variation in morphology and dominant tempering temperature ranges between ε-carbide and cementite, two different sets of correlation constants are adopted at low (below 200°C) and high (above 400°C) tempering temperatures.

The brittle cleavage fracture is captured by a model originally proposed by Ritchie, Knott and Rice (RKR) [10]. The RKR model is derived from continuum fracture mechanics and asymptotic solutions by Hutchinson, Rice, and Rosengren (HRR) for the local stress, strain, and displacements ahead of a tensile crack [11,12].

$$K_{IC} \propto \frac{\sigma_f^{(1+n)/2n}}{\sigma_y^{(1-n)/2n}} \sqrt{l_0} \tag{2}$$

where σ_f is a critical fracture stress that is physically larger than the yield strength σ_y, which must be exceeded by the local tensile opening stress directly ahead of the crack over a characteristic distance l_0 to initiate cleavage. l_0 is found to be typically equal to several grain diameters and conform to the spacing between grain boundary void initiating carbide particles [8,10].

A constant 50 μm is used in the calibration and evaluation with proved reasonable agreement. Based on this, the experimental K_{IC} values of martensitic steels at TME range (~300°C), along with σ_y and n calculated by JMatPro®, are substituted in Eq. (2) to back calculate σ_f, which is then linearly correlated to σ_y. Finally, within the transition tempering temperature range, a scale factor is adopted to describe the extent of strain-controlled micro-void coalescence and stress-controlled cleavage.

Validation and evaluation

Extensive K_{IC} data of general steels has been collected for the validation and evaluation of the aforementioned approach. To simplify the problem, the data selection has the following constraints:

(1) HSLA martensitic steels, with solute composition C = 0.25~0.5%, Si<2%, Mn<1.5%, Cr<3%, Ni<3.5%, Mo<1.2% (wt%).
(2) Commercial steels that contain S and P up to 0.02% (wt%).
(3) Initially austenitised (typically between 800-1200°C) and quenched before tempering.
(4) As-quenched or short-term tempered (≤6h), with the maximum tempering temperature of 650°C.

The composition limits set out in (1) are used to avoid the severity of additional solute effect (e.g. Cr and Ni as strong segregation enhancers [13] leading to further loss in K_{IC} such as in H series steels [14,15] at all tempering temperatures). (2) is because the mechanisms built in the model require the existence of impurity elements. (3) is to ensure the dominant matrix phase is martensite, thus avoiding the mixture of phases with different fracture resistance [2]; and minimise the complication of retained austenite, which serves as a crack arrester as

it is tougher than the martensite phase [16] but becomes detrimental upon destabilisation as mentioned before. (4) is to ensure a unique dominant strengthening phase during tempering.

Figure 2 demonstrates the validity of the approach for K_{IC} calculation for a number of quenched and tempered HSLA martensitic steels at room temperature. Different steels are distinguished by the colours and shapes of the data points. Note that many steels in the experiments were not categorised thus are designated as high strength steels (HSS) in the legend. It is found that the majority of the calculated values fall within a 30% limit region from the measured values and follow the slope of the line of the perfect match.

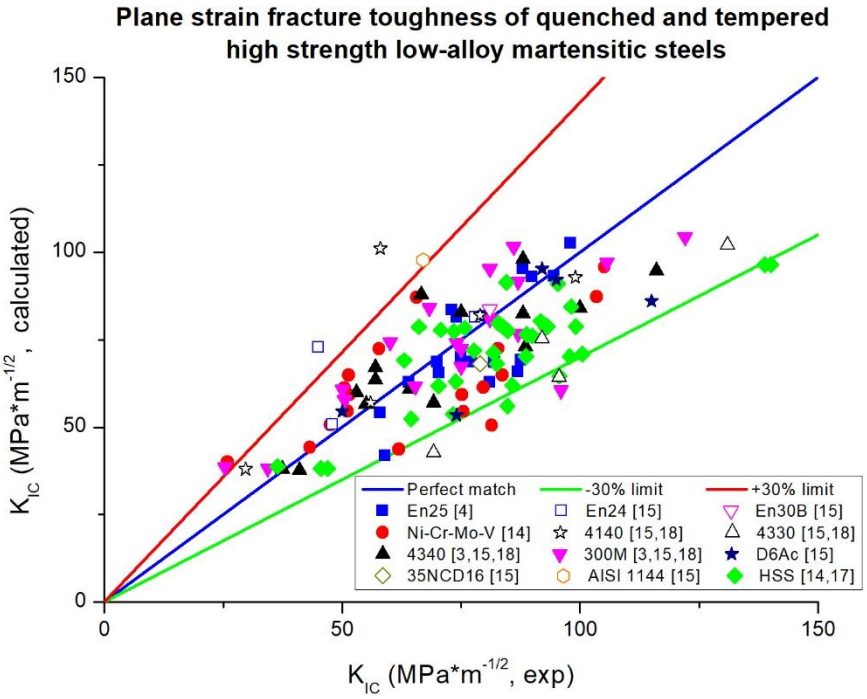

Figure 2 Comparison of calculated plane strain fracture toughness (K_{IC}) of quenched and tempered martensitic steels with experimental measurements at room temperature. In the legend, HSS designates *high strength steels* for the materials in experiments with no specific names.

The variation of the room temperature K_{IC} with tempering temperature for some specific steels is presented in Figs. 3-6, based on the data available in some systematic studies. The initial compositions of these steels are summarised in Table 1. The dashed lines in Figs. 3-6 depict the evolution of the Charpy V-notched impact energy (CVN) as calculated from the popular empirical Barsom-Rolfe upper-shelf correlation [2,19] with the K_{IC} and the yield strength σ_y (Eq.3). Some available CVN data are also shown in these figures.

$$\left(\frac{K_{IC}}{\sigma_y}\right)^2 = 0.65 \cdot \frac{CVN}{\sigma_y} - 0.0065 \tag{3}$$

Table 1 Initial composition (wt%) of the specific steels in some systematic studies of K_{IC}

	C	Ni	Cr	Mo	Mn	Co	Cu	Si	V	P	S	Fe
En25 [4]	0.3	2.55	0.65	0.55	0.55			0.25		0.02	0.02	Bal.
Ni-Cr-Mo-V (1) [14]	0.45	1.72	1.31	0.88	0.44			0.79	0.23	0.012	0.008	Bal.
Ni-Cr-Mo-V (2) [14]	0.44	1.89	1.42	0.96	0.51			0.3	0.26	0.019	0.013	Bal.
HSS1 [14]	0.39	1.46	0.73	0.24	0.13			0.1	0.11	0.005	0.009	Bal.
HSS2 [14]	0.39	3.3	0.75	0.27	1.1	1.05		1.02	0.12	0.005	0.011	Bal.
HSS3 [14]	0.41	3.05	1.5	0.47	0.1			1.07	0.11	0.006	0.012	Bal.
4340 [3]	0.41	1.75	0.79	0.23	0.8		0.06	0.26		0.006	0.004	Bal.
300M [3]	0.42	1.76	0.76	0.41	0.76			1.59	0.1	0.007	0.002	Bal.

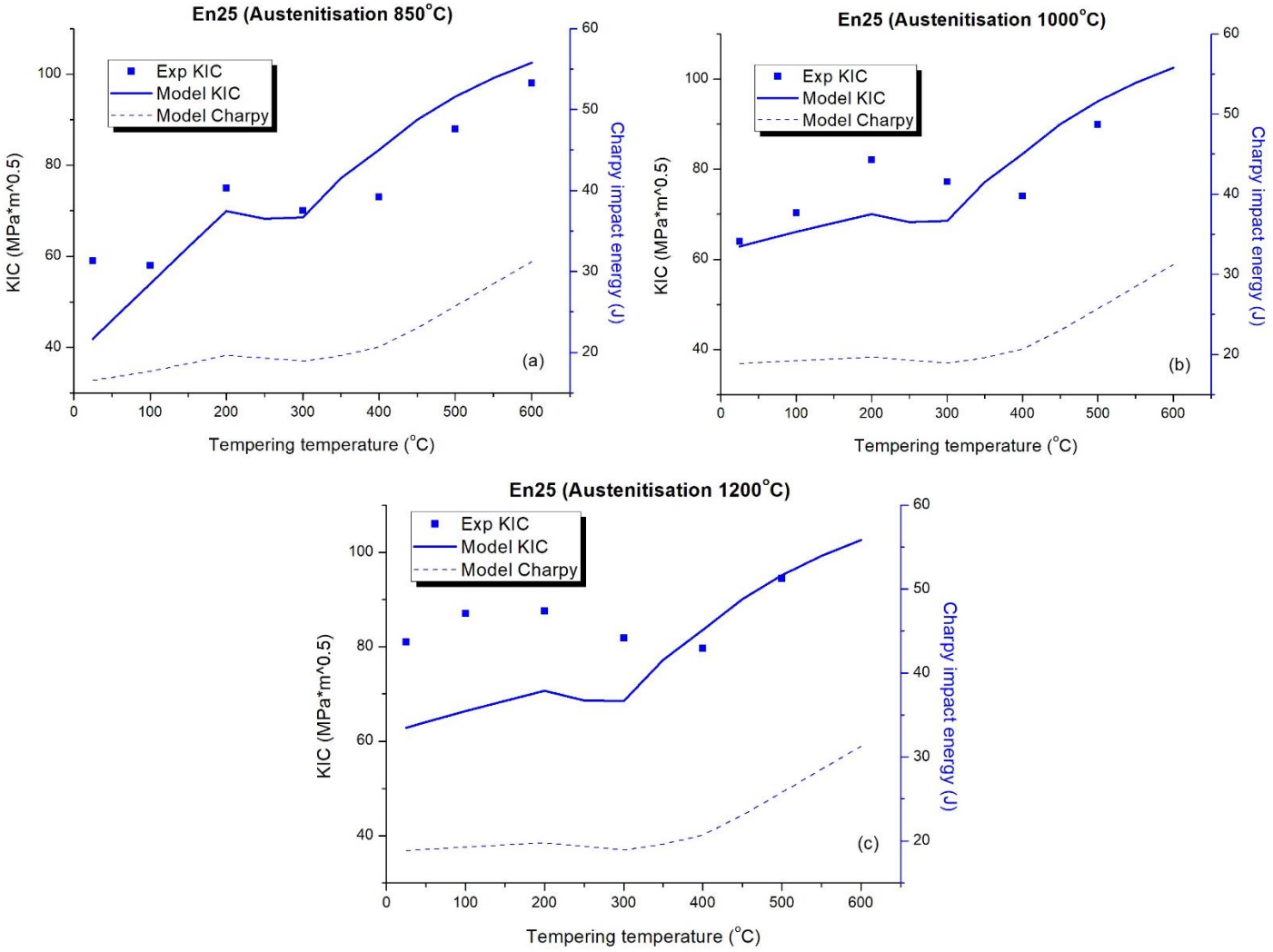

Figure 3 Comparison of calculated and measured variation of the room temperature K_{IC} and Charpy impact energy of ***En25*** with tempering temperature (each with 1 h tempering period), subjected to an initial austenitisation at (a) 850°C, (b) 1000°C and (c) 1200°C.

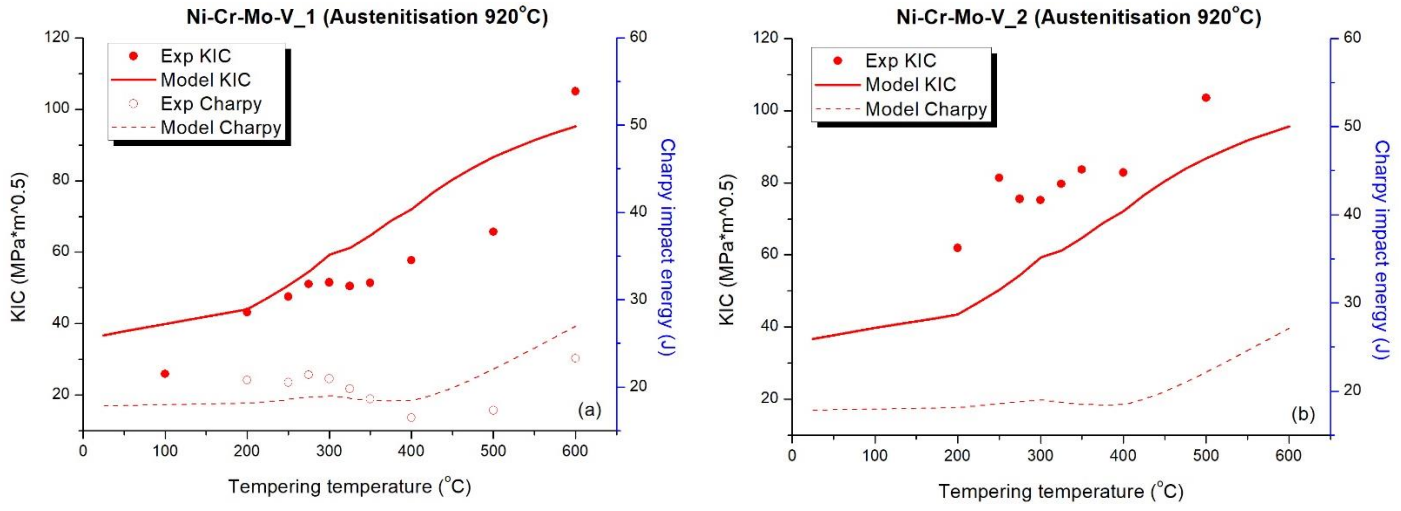

Figure 4 Comparison of calculated and measured variation of the room temperature K_{IC} and Charpy impact energy of two **Ni-Cr-Mo-V** steels with tempering temperature (each with 1 h tempering period), subjected to an initial austenitisation at 920°C.

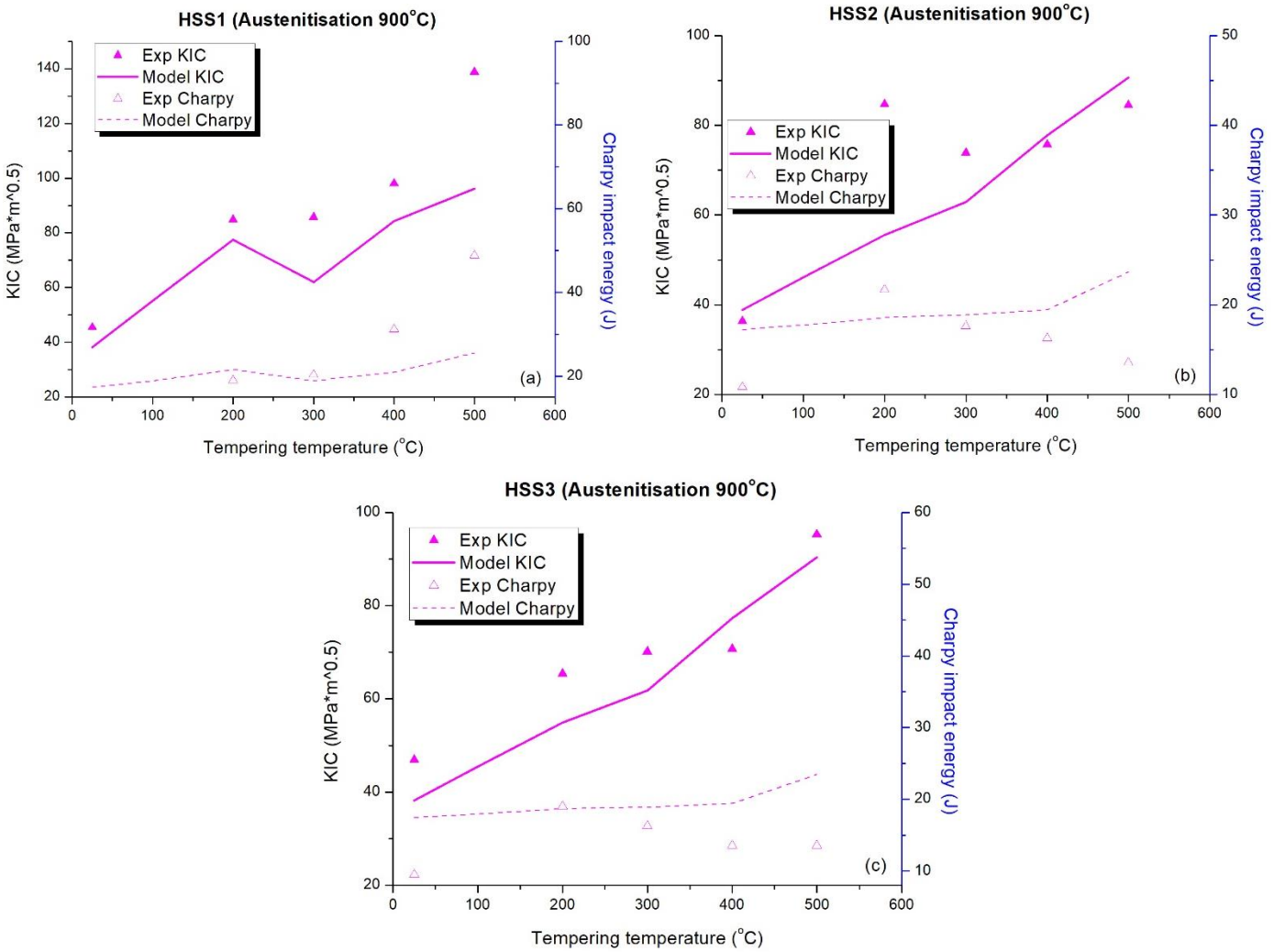

Figure 5 Comparison of calculated and measured variation of the room temperature K_{IC} and Charpy impact energy of three **high strength steels (HSS1-3)** with tempering temperature (each with 1 h tempering period), subjected to an initial austenitisation at 920°C.

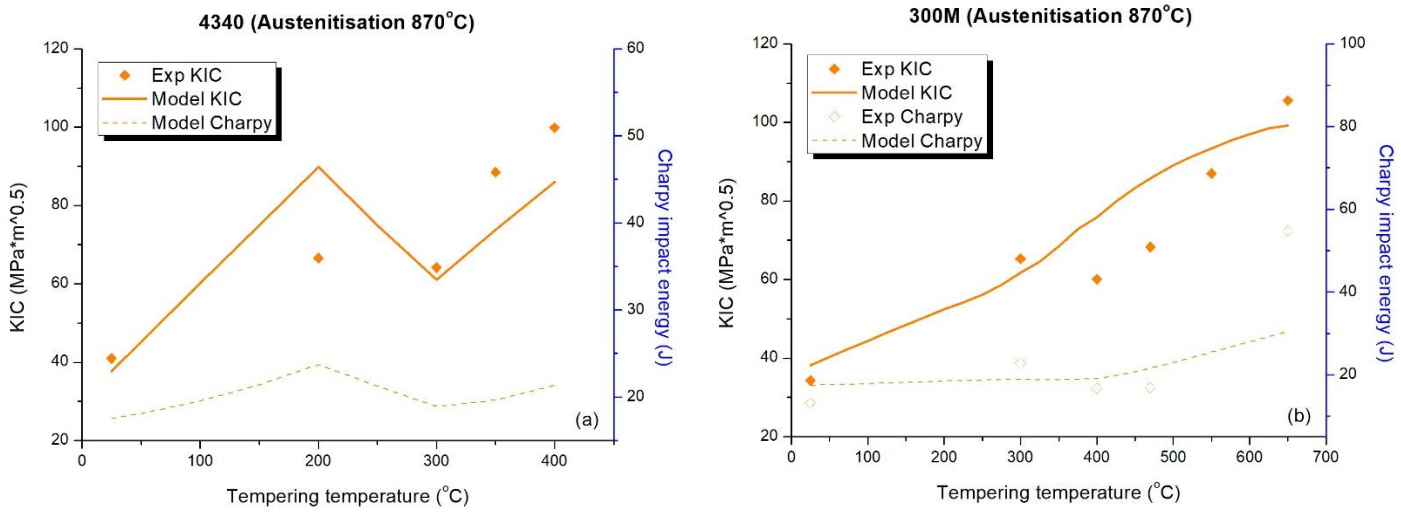

Figure 6 Comparison of calculated and measured variation of the room temperature K_{IC} and Charpy impact energy of (a) **4340** and (b) **300M** with tempering temperature (each with 1 h tempering period), subjected to an initial austenitisation at 870°C.

As can be seen in these figures, the overall trend of the tempering temperature dependence of K_{IC} as well as the Charpy impact energy for these martensitic steels is captured reasonably well. Considering the complexity and intrinsic scatter associated with K_{IC} and impact energy measurements, the agreements provide confidence and robustness in the approach and strategy for K_{IC} simulation proposed in this report.

It is observed that the degree of tempered martensite embrittlement (TME) varies with the material, with some exhibiting a trough while others showing just a plateau around 300°C. The presence of embrittlement is clearly captured in the simulated results for most steels, while for others, such as HSS2-3 and 300M, it is not obvious, but a transition in mechanism can still be observed and the corresponding K_{IC} values are still well within the 30% limit. It is further noted that for En25 austenitised at 1000°C and 1200°C and 300M, the trough seems to have shifted from 300°C to 400°C, or alternatively the occurrence of embrittlement is delayed.

For En25, on one hand, high austenitisation temperatures tend to produce large prior austenite grain size, while on the other hand, the content of impurity elements (Table 1) is seen to be much higher than that in other steels. Both factors may lead to a higher degree of embrittlement given higher tempering temperatures or additional tempering periods sufficient for the impurity elements to diffuse to the prior austenite grain boundary [4]. For 300M, it has a much higher content of Si compared with other steels (Table 1), which is understood to be able to delay the destabilization of the retained austenite [2]. However, these subtle effects have not been quantified and modelled yet.

Summary

Two models, introduced in JMatPro® v11, have been described for determining the room temperature plane strain fracture toughness K_{IC} of quenched and tempered HSLA martensitic steels. Both models link K_{IC} with ordinary tensile properties and different microstructural features including strengthening precipitate phases and impurity elements. The correlation with microstructures reveals and also agrees that a reduction in impurities, precipitate volume fraction and an increase in particle spacing represents an intrinsic toughening process. A combination of the two models is necessary to capture the fracture mechanism transition from cleavage at tempered martensite embrittlement (TME) region to micro-void coalescence at higher tempering temperatures. Reasonable agreement with the available experimental K_{IC} and Charpy V-notched impact energy results has been achieved. The methodology can mitigate the lack of material data required for fracture process simulations and ultimately aid the materials processing and structural integrity assessment.

References

[1] G.T. Hahn, A.R. Rosenfield. Sources of fracture toughness: the relation between KIC and the ordinary tensile properties of metals. Applications Related Phenomena in Titanium Alloys, ASTM STP 432, American Society for Testing and Materials. 1968, 5-32.

[2] R.W. Hertzberg. Deformation and fracture mechanics of engineering materials. Fourth edition. John Wiley & Sons, Inc. 1996.

[3] R.M. Horn, R.O. Ritchie. Mechanisms of tempered martensite embrittlement in low alloy steels. Metallurgical Transactions A. 1978, 9A: 1039-1053.

[4] N.E. Clark. The effect of microstructure on the fracture toughness of a high strength steel. DPhil thesis at University of Auckland, New Zealand. 1976.

[5] T.B. Cox, J.R. Low. Investigation of plastic fracture of AISI-4340 and 18 nickel-200 grade maraging steels. Metallurgical Transactions. 1974, 5(6): 14571470.

[6] A.J. Birkle, R.P. Wie, G.E. Pellissier. Analysis of plane-strain fracture in series of 0.45C-Ni-Cr-Mo steels with different sulfur contents. ASM Transactions Quarterly. 1966, 59(4): 981-990.

[7] Y. Ohmori, I. Tamura. Epsilon carbide precipitation during tempering of plain carbon martensite. Metallurgical Transactions A. 1992, 23(10): 2737-2751.

[8] R.O. Ritchie, A.W. Thompson. On macroscopic and microscopic analyses for crack initiation and crack growth toughness in ductile alloys. Metallurgical Transactions A. 1985, 16A: 233-248.

[9] J. Friedel. Dislocations. Reprinted with corrections ed. Oxford, Reading, Mass: Pergamon; Distributed in USA by Addition-Wesley Pub. Co; 1964.

[10] R.O. Ritchie, J.F. Knott, J.R. Rice. On the relationship between critical tensile stress and fracture toughness in mild steel. Journal of Mechanics and Physics of Solids. 1973, 21: 395-410.

[11] J.W. Hutchinson. Singular behaviour at the end of a tensile crack in a hardening material. Journal of the Mechanics and Physics of Solids. 1968, 16(1): 13-31.

[12] J.R. Rice, G.F. Rosengren. Plane strain deformation near a crack tip in a power-law hardening material. Journal of the Mechanics and Physics of Solids. 1968, 16(1): 1-12.

[13] C.L. Briant, S.K. Banerji. Intergranular failure in steel: the role of grain-boundary composition. International Metals Reviews. 1978, 23(1): 164-199.

[14] Fracture toughness of high-strength materials: theory and practice (ISI publication 120). Iron the Steel Institute. 1970.

[15] Plane strain fracture toughness (KIC) data handbook for metals. Army Materials and Mechanics Research Center. National Technical Information Service. 1973.

[16] D. Webster. Increasing toughness of martensitic stainless steel AFC 77 by control of retained austenite content ausforming and strain aging. ASM Transactions Quarterly. 1968, 61(4): 816-828.

[17] C. Vishnevsky. Effect of alloying elements on tempered martensite embrittlement and fracture toughness of low alloy high strength steels. Final Report for Army Materials and Mechanics Research Center. 1971.

[18] W.E. Wood. Effect of heat treatment on the fracture toughness of low alloy steels. Engineering Fracture Mechanics. 1975, 7: 219-234.

[19] J.M. Barsom, S.T. Rolfe. Correlations between K_{IC} and Charpy V-Notch test results in the transition-temperature range. ASTM STP. 1970, 466: 281-302.